Influence of air chambers on wavefront steepening in railway tunnels

Liu, Feng; Vardy, Alan E.; Pokrajac, Dubravka

Published in:
Tunnelling and Underground Space Technology

DOI:
10.1016/j.tust.2021.104120

Publication date:
2021

Influence of air chambers on wavefront steepening in railway tunnels

Feng LIU [a], Alan VARDY [b], Dubravka POKRAJAC [c]

[a] *School of Engineering, University of Aberdeen, UK*
E-mail: lf198187@163.com
Permanent address:
College of Mechanical and Vehicle Engineering, Taiyuan University of Technology, China,

[b] *University of Dundee and Dundee Tunnel Research, UK*
E-mail address: a.e.vardy@dundee.ac.uk

[c] *School of Engineering, University of Aberdeen, UK*
E-Mail: d.pokrajac@abdn.ac.uk

Corresponding author:

Alan VARDY, Dundee Tunnel Research, Kirkton, Abernyte, Perthshire PH14 9SS, Scotland, UK.
Tel.: +44 1828 686 241
E-mail address: a.e.vardy@dundee.ac.uk

ABSTRACT

The behaviour of wavefronts propagating in a tunnel with multiple, compact air chambers is investigated with particular reference to the suppression of unacceptable pressure disturbances radiating from exit portals. Attention is focussed primarily on chambers that respond in an over-damped manner to pressure variations in the tunnel. In the early part of the paper, comparisons are made between the qualitative behaviour of wavefront propagation in tunnels with and without air chambers. Thereafter, attention turns to a quantitative assessment of the influence of key design parameters, especially the chamber volume and properties of connectors between chambers and the tunnel. It is shown that the optimum type of connector depends upon the length of the tunnel along which the chambers exist. For short tunnels, relatively low-resistance connectors with linear pressure:flow rate characteristics are preferred, whereas for long tunnels, relatively high-resistance

connectors with quadratic pressure:flow rate characteristics are likely to be more suitable. Brief attention is paid to the practical feasibility of creating suitable connectors.

Keywords

Wavefront steepening, rail tunnels, air chambers, micro-pressure waves

NOMENCLATURE

1-D	one dimensional
3-D	three dimensional
A	cross-sectional area of tunnel, m^2
a_{acc}	inertial coefficient, -
c	speed of sound, m/s
D_{tun}	effective diameter of tunnel, m
K_1	linear resistance coefficient, s^{-1}
K_{1c}	critical linear resistance coefficient, s^{-1}
K_2	quadratic resistance coefficient, mkg^{-1}
$\dot{m}$	mass flow rate per unit length (positive into chambers), $kg.s^{-1}m^{-1}$
p	pressure, Pa
R	specific gas constant, J/kg.K
s	variable in the characteristic polynomial (Eq-5), s^{-1}
T	absolute temperature, K
t	time coordinate, s
U	axial velocity (cross-sectional average), m/s
V_R	Volumetric ratio chambers:tunnel
V	Chamber volume per unit length, m^2
x	spatial coordinate along tunnel, m

Greek characters

γ ratio of principal specific heat capacities

ρ density, kg/m^3

Subscripts

A,B,L,R local subscripts defined in Fig-4

ch chamber

tun tunnel

1 INTRODUCTION

A range of counter-measures exists to reduce the severity of micro-pressure waves (MPWs) emitted from railway tunnel portals [1,2]. The most common of these is the construction of large entrance regions designed to reduce the steepnesses of nose-entry wavefronts [3-6]. The reduction needs to be sufficiently large to ensure that subsequent wavefront shortening during propagation along the tunnel does not result in waves that are unacceptably steep when they reach the exit portal.

Many other methods of achieving the desired reduction have been investigated. For example, use can be made of airshafts from the tunnel to surface level [7]. Although this has little influence on wavefront lengths [8], it reduces amplitudes and hence steepnesses. Multiple shafts can reduce final steepnesses to acceptable levels. Other possibilities include the provision of expansion chambers upstream of tunnel exits [9] and the use of active attenuation devices [10].

Pores in a ballast-track bed can greatly reduce the maximum gradients of wavefronts, especially in long tunnels [11,12]. However, due to the complexity of stone particle size distribution, current research and understanding of ballast is insufficient for practical design. Also, the suitability of gravel track beds on high-speed railways is restricted by factors such as maintenance requirements and rubble splash.

A widely used countermeasure, especially in Japan, is to extend train nose lengths [13-15]. However, the extensions need to be quite long; extensions shorter than about one tunnel diameter give relatively small benefit. Another possibility is to reduce train speeds for a few seconds during train entry to tunnels, noting that the steepness of nose-entry wavefronts varies approximately with the cube of the train entry speed. Unfortunately, operators resist this method for reasons unrelated to aerodynamics.

It would be desirable to have an effective in-tunnel counter-measure, thereby avoiding visual and practical inconvenience outside portals. One such possibility was introduced by Sugimoto [16] and, in a different form, by Tebbutt et al [17]. These methods make use of Helmholtz resonators that hamper the transmission of higher frequencies in wavefronts. They are potentially well suited to attacking acoustic frequencies and thereby mitigating the consequences of MPWs. However, Tebbutt et al concluded that realistic arrays of Helmholtz resonators are unlikely to be a sufficient counter-measure on their own. Another in-tunnel method of suppressing MPWs has been installed retrospectively in newly constructed tunnels when moderate, but nevertheless undesirable, MPWs were in the audible range [18]. It is not known whether this method, namely the installation of sound absorbers loosely akin to acoustic linings in ducts, would be a practical counter-measure in more severe cases. Sasoh et al [19] demonstrated experimentally the advantages of a large, enclosed space behind the sound-absorber material. In the measured case, this space was continuous along the duct and its cross-sectional area exceeded that of the duct. A loosely similar geometry is considered herein, but the enclosed space is not axially-continuous and its cross-sectional area is small in comparison with that of the tunnel.

The principal purpose of this paper is to assess the influence of a continuous array of purpose-designed air-storage chambers along a tunnel (Fig-1a) on the steepness of wavefronts arriving at an exit portal. The aim is to ensure that the ultimate steepness is below the value that would cause the emission of unacceptable MPWs. The proposed chambers have much in common with Helmholtz

resonators, but there is a crucial difference, namely that they are designed *not* to resonate. Instead, they induce behaviour similar to that of wavefront propagation in ballast track tunnels [20,21], causing wavefronts to elongate, not shorten. The key difference from typical Helmholtz resonators is that the connections between the chambers and the tunnel ensure that flows through them are dominated by resistance and result in 'over-damped' behaviour. Figure-1b illustrates a possible configuration of the connections between a chamber and a tunnel. Many other configurations will be possible, but it is likely that all will have multiple flow paths, each of small cross-section. This will be necessary to achieve the overall resistance properties that the following analysis shows will be required.

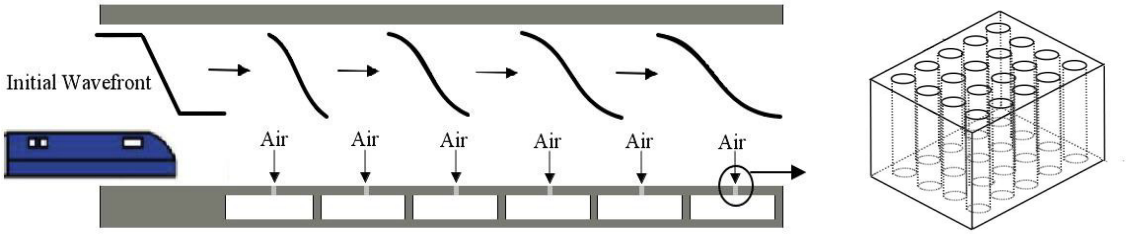

(a) Chambers (b) Connectors

Fig-1 Schematic illustration of wavefront elongation caused by air-storage chambers (Fig 1b is merely indicative of one possible form of connectors)

The following Section focusses on the air chambers and connections and how their key properties influence the nature of their responses to external variations in pressure. Then, attention turns to the analysis of wavefront propagation along a tunnel and to how the analysis thereof is combined with the analysis of the air chambers. Section-4 assesses performance in detail, with particular reference to parameters that might be available to tunnel designers and also to the sensitivity to wavefront amplitudes. In most of the discussion, the connector resistance is deemed to depend linearly on velocity, but consideration is also given to non-linear resistance. Two Sections are then devoted to practical matters related to design and key points are summarised in a concluding Section.

2 AIR CHAMBERS AND CONNECTIONS

For the purposes of this paper, the air chambers are assumed to be distributed uniformly over long lengths of tunnel, possibly, but not necessarily, the whole length. The practicality of this is discussed in Section 5. Their shape is unimportant, but their volume is of high importance, as also are the properties of the connections between the chambers and the tunnel. Many different types of connector are possible, including continuous (narrow) slots or numerous discrete holes for example. However, the emphasis herein is on properties such as flow resistance, not on alternative ways of causing such resistance.

It is assumed that the chambers are isolated from one another, thereby preventing axial flow between them along the tunnel. This is because their effectiveness depends upon entrapping air that would otherwise contribute to the steepening process of wavefront propagation. Axial inter-connections would certainly have an influence – as found in studies of ballast track tunnels [20] – but it is unlikely to be beneficial.

2.1 Flow through the connectors

The pressure difference ($p_{tun} - p_{ch}$) between the tunnel and the chambers depends upon $\dot{m}$, the mass flow rate per unit length of tunnel into the chambers and upon its rate of change d$\dot{m}$/dt. The momentum equation can be written as:

Momentum:
$$p_{tun} - p_{ch} = K_1 \dot{m} + K_2 \dot{m}|\dot{m}| + a_{acc} \frac{d\dot{m}}{dt} \qquad (1)$$

in which K_1 and K_2 are coefficients defining the resistance of the connection, t is the time coordinate, and a_{acc} is an inertial coefficient. For the particular geometry illustrated in Fig-1b, a_{acc} is equal to the ratio of (i) the effective length of the connectors, including a small allowance for end effects and (ii) the cross-sectional area of flow per unit length through the connectors. In the following analytical development, each of these coefficients is implicitly regarded as a constant, although this does not preclude them having different values in successive time steps in the numerical solution process. For example, the resistance coefficients might be Reynolds-number dependent.

The continuity equation for flow into the chambers is

Continuity:
$$\frac{d(\rho_{ch}\forall)}{dt} = m \tag{2}$$

in which $\forall$ is the chamber volume per unit length and ρ_{ch} is the density of air in the chamber. Assuming that pressure changes in the chamber occur almost isentropically in the tiny timescales under consideration, the rate of change of pressure in the chamber will be given by

$$\frac{dp_{ch}}{dt} = \frac{\dot{m}c_{ch}^{\,2}}{\forall} \tag{3}$$

in which c_{ch} is the isentropic speed of sound in the chamber. The air is simulated as a perfect gas so the speed of sound can be expressed either as $(\gamma p/\rho)^{½}$ or as $(\gamma RT)^{½}$, where γ is the ratio of the principal specific heat capacities, R is the specific gas constant and T is the absolute temperature. Over much larger time scales than those considered herein, heat transfers with the walls of the chambers will cause pressures in the chambers to migrate towards conditions resembling isothermal behaviour. However, this process will occur gradually and it will have negligible influence on early responses to very rapid pressure changes.

In the computer program used to derive results presented below, Eqs 1 & 3 are integrated numerically over short time steps Δt and are solved simultaneously with wave equations presented below. This is done iteratively. It is worth noting in passing that Eq-3 shows that a *constant* rate of mass flow into a chamber would cause a continual increase of pressure in the chamber and Eq-1 shows that this would imply that the pressure in the tunnel is rising at a similar rate – e.g. when a wavefront passes alongside a chamber. After such a wavefront has passed, the pressure in the tunnel is approximately constant and so the rate of flow into the chamber will reduce as the pressures gradually equalise.

2.2 Generic behaviour

Before linking the above analysis to the analysis of wave propagation along a tunnel, it is useful to explore the implications of the above equations for the generic behaviour of chambers in response to imposed changes in external pressure. Differentiating Eq-1 with respect to time and using Eq-3 to eliminate dp_{ch}/dt leads to

$$a_{acc}\frac{d^2\dot{m}}{dt^2}+(K_1+2K_2|\dot{m}|)\frac{d\dot{m}}{dt}+\frac{\dot{m}c_{ch}{}^2}{V}=\frac{dp_{tun}}{dt} \qquad (4)$$

It is instructive to consider the special case of dp_{tun}/dt=0, which is a close approximation to conditions after a sudden change in pressure in the tunnel. When consideration is further restricted to the case of linear resistance (i.e. K_2 = 0), the homogeneous part of this differential equation has a characteristic polynomial that can be written as

$$a_{acc}s^2+K_1s+\frac{c_{ch}{}^2}{V}=0 \qquad (5)$$

When both roots of this equation are real, the chamber behaves in an over-damped manner. When they are imaginary, it behaves in an under-damped manner. The intermediate condition of critical damping exists when K_1 is equal to a critical value K_{1C} that satisfies

Critical damping:
$$K_{1C}=2c_{ch}\left(\frac{a_{acc}}{V}\right)^{0.5} \qquad (6)$$

When $K_1 > K_{1C}$, the chamber is over-damped and, when $K_1 < K_{1C}$, it is under-damped.

The three types of behaviour are illustrated schematically in Fig-2. Figure-2(a) shows possible pressure variations in the chamber in response to a rapid, step-change in pressure in the tunnel. The broken lines show oscillatory behaviour typical of under-damped chambers. The thick continuous line represents a critically damped case for which oscillations are just prevented and the thin continuous line shows stronger damping. Figure-2(b) compares different resistances in a qualitative manner. Once again, the thick continuous line denotes critical linear resistance. The whole of the region above this line corresponds to over-damping and the region below it corresponds to under-

damping (e.g. the line labelled $K_1 < K_{1c}$). The two curved lines labelled "Small K_2" and "Large K_2" depict quadratic resistances. For both of these, the behaviour at low rates of flow is under-damped whereas that at larger rates of flow is over-damped. More-over the degree of over-damping increases rapidly with increasing flow rate. Some consequences of this are explored in Section 4.5 below.

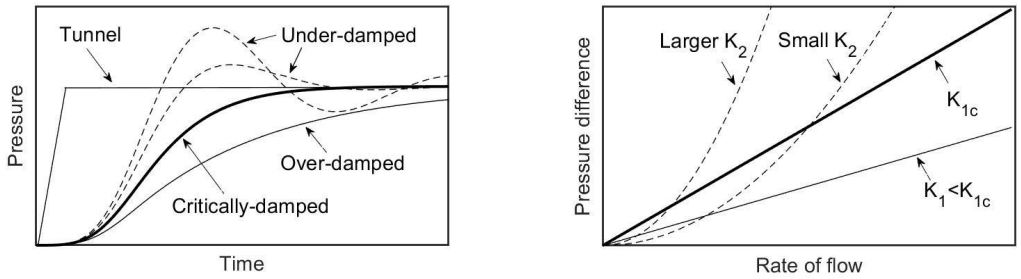

(a) Response to change in external pressure (b) Influence of resistance characteristics

Fig-2 Over-damped, under-damped and critically-damped behaviour

2.3 Indicative influence of chambers on a wavefront

Figure-3 illustrates conditions at a typical instant during the propagation of a wavefront along a region of tunnel containing air chambers. The thin lines show pressure distributions in the tunnel and in the chambers, and the thick continuous line shows the difference between them. Close to the toe and heel of the wavefront, the pressure differences are small and, as illustrated in Fig-2(b), the response with non-linear connectors will be under-damped. At intermediate locations along the wavefront, however, the differential pressure is greater and so over-damped responses can be possible even with the non-linear connectors. This is of high importance because the chambers exert greatest influence when the differential pressures are large. It is highly desirable for this condition to coincide with the periods when the incident wavefront is steepest – as in the example in Fig-3.

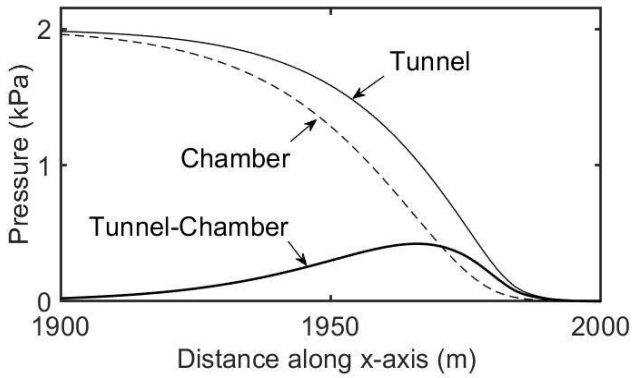

Fig-3 Typical pressure distribution along a wavefront in a tunnel with air chambers

3 WAVEFRONT PROGPAGATION

The analysis of wave propagation along the tunnel is simulated herein using one-dimensional approximations. In part, this is because it is appropriate to use the simplest methodology that will yield acceptable accuracy, noting that plane wave assumptions will closely approximate reality when the air-chambers fulfil their purpose of preventing steep wavefronts. This enables large numbers of simulations to be undertaken, leading to a comprehensive assessment of all key parameters. Furthermore, it would not be practicable for flows through large numbers of small-area connectors to be represented in detail in 3-D simulations designed to study wave propagation along several kilometres of tunnel.

The airflows are treated as inviscid even though allowing for friction is straightforward. The advantage of this is that it avoids any risk of misinterpreting the damping caused by chambers as being due to other causes. In practice, additional simulations including friction (not presented herein) have shown that its influence is an order of magnitude smaller than that of the chambers. Naturally, it should be included in a practical engineering design, but its inclusion herein would be unhelpful.

3.1 Governing equations

The equations of continuity and momentum for one-dimensional, inviscid flow along a horizontal tunnel between successive connectors

Continuity: $$\frac{\partial \rho}{\partial t} + U\frac{\partial \rho}{\partial x} + \rho\frac{\partial U}{\partial x} = 0 \quad (7)$$

and

Momentum: $$\frac{\partial p}{\partial x} + \rho\frac{\partial U}{\partial t} + \rho U\frac{\partial U}{\partial x} = 0 \quad (8)$$

in which ρ and p are the density and pressure, U is the axial air velocity, x is the distance along the tunnel and t is time.

Using the Method of Characteristics (MOC), these equations can be recast as a pair of ordinary differential equations:

MOC Equations: $$\frac{dp}{dt} \pm \rho c\frac{dU}{dt} = 0 \quad (9)$$

that are valid along families of characteristic lines with gradients that everywhere satisfy

MOC directions: $$\frac{dx}{dt} = U \pm c \quad (10)$$

respectively, in which the speed of sound, c, satisfies

Sound speed: $$c^2 = \frac{dp}{d\rho} = \frac{\gamma p}{\rho} \quad (11)$$

In many analyses of unsteady flows in pipes and ducts, the convective terms in the continuity and momentum equations are discarded and the MOC directions then reduce to $dx/dt = \pm c$. This

simplification would not be acceptable herein because the convective terms are the ones that cause the inertial steepening that the air-chambers are designed to counteract.

3.2 Numerical integration

The grid structure used for the numerical integration of the above equations is depicted in Fig-4. Each calculation node has a double grid point at which the velocity changes abruptly (because of the lateral flows), but the pressure and density are regarded as continuous.

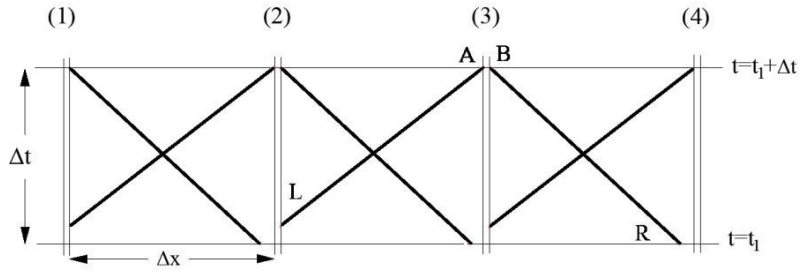

Fig-4 Numerical grid structure
The gradients of the characteristic lines are U±c

The numerical solution proceeds in a time-marching manner in which the solution is obtained at all locations at the time t_1 before a solution is sought at the time $t_1 + \Delta t$. For the single-wavefront cases of interest herein, the dominant direction of propagation is known *a priori* (from left to right in Fig-4) and the solution mirrors this by obtaining solutions in the sequence (1), (2), (3)... Thus, for instance, the solution at location (2) is obtained before solving the equations for location (3). As a consequence, values at L can be interpolated along the time-line through L. The corresponding values at R are obtained by spatial interpolation at the time t_1. In both cases, linear interpolation is used and the gradients of LA and RA are approximated by simple averages of $U \pm c$ at their end points. The need for interpolation arises because the gradients of the characteristic lines are not treated as universal constants (see above) even though a fixed grid structure is used. However, the locations of L and R also depend on the chosen grid shape. The particular locations shown in Fig-4 are indicative of grid shapes corresponding to Courant numbers close to unity.

Using the nomenclature in Fig-4, integration of the MOC equations in the characteristic directions gives

Along LA: $$(p_{AB} - p_L) + (\rho c)_{LA}(U_A - U_L) = 0 \quad (12)$$

and

Along RB: $$(p_{AB} - p_R) - (\rho c)_{RB}(U_B - U_R) = 0 \quad (13)$$

In which the products $(\rho c)_{LA}$ and $(\rho c)_{RA}$ are average values along the respective characteristic lines and the pressure is treated as continuous at AB, even though the velocity is discontinuous when a connection to a chamber exists at the grid point. Strictly, it would be more correct to regard the stagnation pressure as continuous (i.e. not the static pressure), but this would complicate the solution process whilst yielding negligible increase in accuracy. At Mach numbers relevant to the present study, changes in $\frac{1}{2}\rho U^2$ due to due to small differences between U_A and U_B are tiny in comparison with wave-induced pressure changes described by Eq.13.

The influence of the chambers is described by Eqs 1 & 3, which are approximated numerically as

$$p_{AB} - p_{ch} = K_1 m_{av} + K_2 (m|m|)_{av} + a_{acc} \frac{m - m_{t-\Delta t}}{\Delta t} \quad (14)$$

and

$$\frac{p_{ch} - p_{ch,t-\Delta t}}{\Delta t} = \frac{m_{av} c_{ch,av}^2}{V} = \frac{m_{av} (\gamma p/\rho)_{ch,av}^2}{V} \quad (15)$$

in which the suffix *av* denotes an average over the integration time step Δt and parameters with no temporal suffix are applicable at the solution time t.

The MOC equations 12 & 13 are coupled to the chamber equations 14 & 15 by a continuity equation that relates the velocity difference ($U_A - U_B$) to the rate of flow through the connection, namely

$$\rho_{AB} A (U_A - U_B) = \int \dot{m} dx \tag{16}$$

where *A* is the cross-sectional area of the tunnel and $\int \dot{m} dx$ is the total mass flow rate through all connections simulated at the grid point. When the connections are represented as a uniform slot along the tunnel, $\int \dot{m} dx = \dot{m} \Delta x$ at each grid point. When they are treated as discrete holes at regular intervals, each hole is allocated to its nearest grid point and $\int \dot{m} dx = 0$ at intermediate points.

In each time step, the five equations 13-17 are solved at each grid point in turn to yield values of the five principal unknowns, namely the pressures p_{AB} & p_{ch}, the velocities U_A & U_B and the mass flow rate $\dot{m}$. The solution process is iterative. First, an estimated value of $\dot{m}$ is used in Eq-16 to provide a corresponding estimate of p_{ch}. This value is then treated as a constant in Eq-15 which is solved together with Eqs-13, 14 & 17 to give estimates of revised estimates of p_{AB}, U_A, U_B and an improved estimate of the mass flow rate $\dot{m}$. The process is then repeated until successive estimates of $\dot{m}$ differ by less than a convergence tolerance of 10^{-4} kg/s. It has been confirmed that the use of tighter tolerances has negligible influence on the calculated results. In addition to solving Eqs. 13-17, the iterative process includes updating the locations of L & R and updating all values that depend on these.

3.3 Grid size dependence

The grid size used for the simulations presented herein is sufficiently small that either an increase or a decrease by a factor of two has negligible influence. This assessment has been made using the steepest wavefront investigated. The insensitivity of grid size ensures adequate *convergence*, but it does not, by itself, guarantee *accuracy* because that also depends upon the shape of the grid (i.e. $c\Delta t/\Delta x$). However, only a small range of values of this ratio needs to be considered because, in

simulations herein, the local values of $c \pm U$ never differ by as much as 2% from the ambient speed of sound c_0. In practice, only negligible differences have been detected when varying $\Delta x / c\Delta t$ by this amount so the same ratio has been used in all simulations, corresponding to $\Delta x / \Delta t = c_0$.

3.4 Validation

The above process confirms that the numerical method gives a close approximation to the solution of the analytical equations even though interpolation is necessary. However, it gives no information about the suitability of the analytical equations themselves. That has to be assessed independently and, in practice, it must be done indirectly because there is no practical way of providing the necessary checks by means of small-scale experiments or 3-D CFD calculations. In both cases, this is prevented by a need to model flows through large numbers of very small diameter connections (e.g. 1 mm diameter) between the tunnel and the chambers as well as along long lengths of tunnel (several kilometres). The authors have plans to undertake CFD studies to determine whether the time needed for waves to propagate laterally in the tunnel will be beneficial or otherwise. However, this will be done using user-defined functions to represent flows through the connectors in a similar manner to that used in the present analysis (i.e. Eqs 15-16). Therefore, it will, at best, be of limited value for the purposes of validation. Likewise, plans exist for building a laboratory model to measure the influence of chambers. However, this too will not provide direct validation because there is no practical method of scaling vast numbers of short, small diameter connectors. Instead, the model will have to be used in a different flow regime from the proposed full-scale case.

An indirect validation of the methodology has been undertaken during a preliminary investigation of the potential of air-storage chambers in which special attention was paid to the asymptotic states of wavefronts. Liu et al [22] compared predictions from the above model with predictions presented by Vardy & Brown [21] in a study of wave propagation in ballast-track tunnels. They imposed various linear increases in pressure at one end of a tunnel and tracked the evolution of the resulting wavefront along the tunnel. As shown in Fig-5, the two sets of predictions are sufficiently close for confidence to be placed in them both. Nevertheless, differences exist, notably before the chambers

have exerted their full influence on the steepest of the four wavefronts considered. Although not provable, it seems highly likely that the present results are the more accurate of the two. In part, this is because the earlier methodology is believed to have used a one-step predictor-corrector integration, whereas a fully-convergent iterative process is used herein. The asymptotic state labelled in the figure is discussed after considering further details shown in Fig-6.

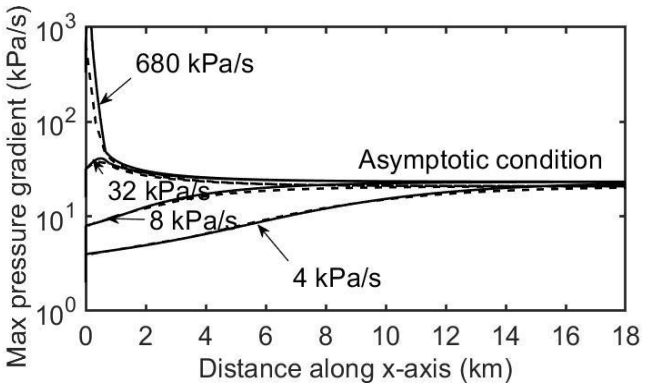

Fig-5 Comparison with predictions by Vardy & Brown [21] (dashed lines).

4 QUANTITATIVE BEHAVIOUR

Attention now turns to quantifying the ability of air chambers to suppress wavefront steepening. First, a base case is used to highlight key features and an important dependence on wavefront amplitude is demonstrated. Then the influence of the chamber volume and the connection properties is assessed. For this purpose, it is more useful to consider the total volume of chambers in a given length of tunnel than the volume of any individual chamber. Accordingly, a chamber:tunnel volumetric ratio, V_R, is introduced, defined as the ratio of the total volume of chambers in any given length to the volume of the same length of tunnel.

4.1 Base case

In all of the following simulations, the chamber:tunnel volumetric ratio, V_R, is uniform along the simulated region of tunnel and, except in Section 4.5, the connection resistance is linear. In the base case, V_R = 3%, the critical resistance given by Eq.7 is K_{1C} = 500 $m^{-1}s^{-1}$ and the actual resistance K_1 = 1000 $m^{-1}s^{-1}$, corresponding to K_1/K_{1c} = 2. Ambient initial conditions are disturbed by a wavefront that causes a prescribed pressure history at the upstream end of the simulated region. The history,

which is shown by continuous lines in the left-hand boxes of Figs-6(a) & 6(b), has an 'S' shape that is broadly indicative of typical nose-entry wavefronts [23]. The detailed predictions presented below are specific to this particular shape, but this is a much smaller limitation than it appears at first sight. Vardy & Brown [21] showed that, for the related case of propagation over a ballast track, all wavefronts of equal overall amplitude will migrate towards a common asymptotic shape, regardless of whether they are initially steeper or less steep than the asymptote. This effect is seen in Fig-5 above. As a consequence of this behaviour, the most important characteristic of wavefronts in the present contest is their maximum steepness, not their overall shape. Accordingly, it is considered acceptable to focus on a single generic shape and to explore the influence of steepness by varying the overall amplitude.

The broken lines in Fig-6 show two possible interpretations of the pressure gradient. One is the usual mathematical definition. The other is a 'smoothed' gradient that is more relevant to the end use of the analyses, namely the prediction of MPW amplitudes. It allows for time delays in the reflection/radiation process when a wavefront reaches a tunnel exit portal [24-25]. The smoothed value is the gradient of a chord over a time interval of $0.6D_{tun}/c$, where D_{tun} denotes the effective diameter of the tunnel cross-section. The adjustment corresponds to twice the time required for a wave to travel between the true portal plane and an effective reflection plane a small distance outside it [26-27]. Hereafter, only the smoothed gradients are used and, following the usual practice, these are usually referred to as 'steepnesses'.

The wavefront amplitude is 2 kPa so the velocity at the maximum pressure is approximately 5 m/s greater than that at its toe. Likewise, the speed of sound at the heel is approximately 1 m/s greater than that at the toe. As a consequence, in the absence of chambers, the whole wavefront shortens continuously at a rate of approximately 6 m/s, causing the steepening shown in Fig-6(a). In contrast, when the chambers exist – Fig-6(b) – the maximum steepness reduces slightly.

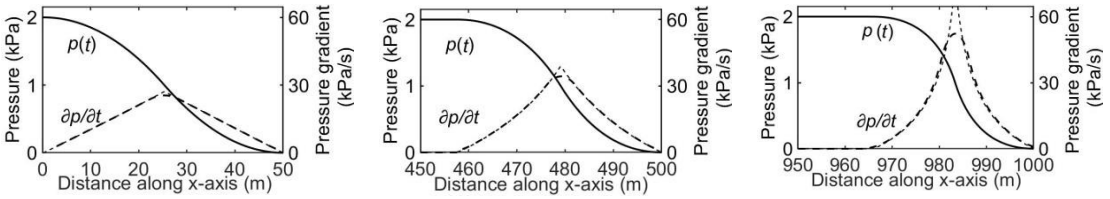

(a) Tunnel with no air chambers (wavelength 50m)

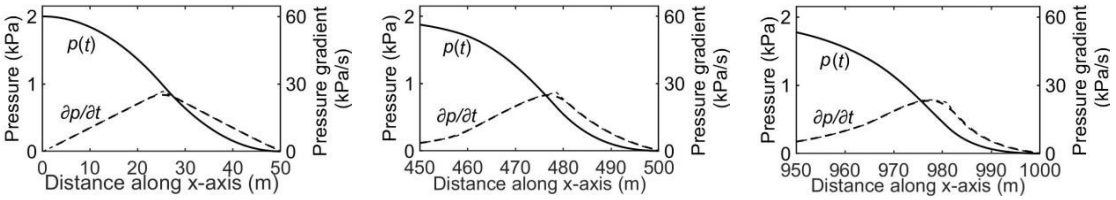

(b) Tunnel with air chambers (wavelength 50m)

Fig-6 Wavefront evolution in tunnels with and without air chambers

after the toe has travelled 50, 500 and 1000 m

[V_R = 3%; K_1 = 1000 s^{-1}**;** K_2 = 0**; K_1/K_{1c} = 2; Initial wavelength = 50m]**

In practice, the reduction in steepness continues indefinitely, but at gradually reducing rates as the wavefront tends towards an asymptotic state. This behaviour is seen in Fig-5, which shows the evolution of the maximum steepnesses of four wavefronts with different initial steepnesses. For this purpose, the steepness is evaluated at all locations and the graphs show the largest value, regardless of its position along the wavefront. In Fig-6(b), the location of the maximum steepness migrates towards the wavefront tip, but migration away from the tip is possible with other chamber and connection properties.

In Fig-5, all four wavefronts tend towards a common asymptote after travelling sufficient far along a line of chambers. Wavefronts that are initially steep approach the asymptote rapidly whereas initially gentle ones do so only slowly. Both of these characteristics are beneficial for the purposes of suppressing MPWs. When the asymptotic state is sufficiently small, the chambers have the potential to eliminate the need for any other form of counter-measure against the risk of unacceptable MPWs. This potential is assessed in the following Sections.

4.2 Wavefront amplitude

Although the asymptotic condition is almost independent of the initial steepness of the wavefront, it does depend on the wavefront amplitude. Figure-7(a) shows the evolution of maximum steepness for 50 m wavefronts with upstream amplitudes maintained as 1 kPa, 2 kPa and 3 kPa respectively. This range brackets values likely to be generated in conventional high-speed railway tunnels during the next few decades. In each case, the chambers have the base case specifications, namely V_R = 3%, K_1 = 1000 $m^{-1}s^{-1}$ and K_1 / K_{1c} = 2. By inspection, they cause the maximum steepness of the 1 kPa wavefront to reduce almost immediately, whereas those of larger wavefronts increase before beginning to reduce. It follows that the base case chambers would be unsuitable for use in short tunnels – although, even for these, the increase in steepness is smaller than in a tunnel with no chambers.

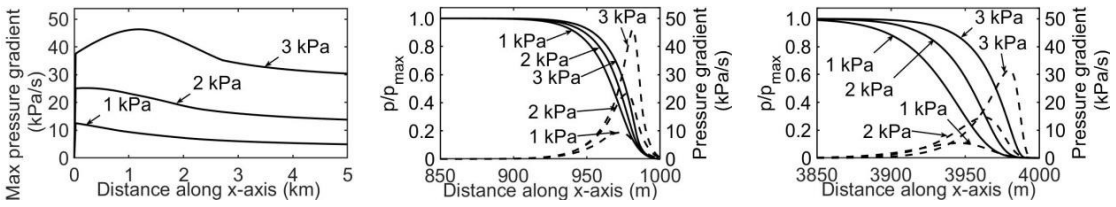

(a) Evolution of maximum gradient (b,c) Instantaneous profiles after 1 km & 4 km

Fig-7 Influence of wavefront amplitude

(V_R = 3%; K_1 = 1000 s^{-1}**;** K_2 = 0; K_1/K_{1c} = 2; 50 m wavefront)

Figures-7(b),(c) show instantaneous profiles of the pressure (continuous lines) and the steepness (dashed lines) in the leading 150 m of the wavefronts after their toes have travelled 1 km and 4 km. To simplify comparisons, the pressures are scaled in proportion to their initial amplitudes, thereby highlighting key features. One obvious feature of the figures is that the proportional reduction in the gradient increases with decreasing wavefront amplitude. It follows that, if the chambers are designed to perform adequately for the maximum expected wave amplitudes, they will be even more effective for all smaller amplitudes. A second feature is that the bulk speed of propagation of the lower amplitude wavefronts is smaller than that of the high amplitude ones. Also, there is a finite region of almost ambient pressure between the apparent (effective) toe of each bulk wavefront and the true toe (which propagates at ambient sonic speed and has travelled exactly 1km

and 4km in Figs-7(b),(c)). The length of this region for any particular wavefront could be regarded as a qualitative measure of the residual capacity of the chambers – i.e. their likely ability to attenuate larger wavefronts of the same shape.

A third feature of the figure, important for academic understanding and for designers, is that, when the wavefront amplitude is sufficiently large (here 3kPa), the loci of the maximum gradients tend to propagate faster than the effective toes, but (except in the early stages of propagation) slower than the theoretical toes. This can be seen directly by inspecting the graphs of rates of change of pressure. However, it is instructive to inspect also the pressure profiles themselves. Their inflection points coincide with their maximum steepnesses and it is seen that, as these points migrate towards the effective toes, the regions ahead of them become shorter and steeper. By inference, the leading parts of even greater amplitude wavefronts than those considered in Fig-7 could potentially evolve into shocks (or very nearly so). In this context, note that, in the absence of the chambers (and friction, etc), the whole of the initial 3 kPa wavefront would develop into a shock in less than 3 km.

4.3 Chamber:tunnel volume ratio

The chamber:tunnel volume ratio is an important parameter. Larger chambers can capture more air and hence have greater potential for flattening wavefronts than do smaller chambers. However, practical and financial constraints limit freedom of choice in this respect. The maximum value considered herein is 5%. Figure-8 shows the evolution of the base case wavefront for chambers with volume ratios from 1% to 5%. To preserve the relative importance of inertial and resistive effects, the comparisons are based on identical values of the ratio K_1/K_{1c}, namely 2. For this purpose, K_{1c} is calculated first, using Eq-7. Then, K_1 is then chosen as $2K_{1c}$.

Figure-8(a) shows the evolution of the maximum wavefront steepness. All five cases constrain the steepening process, but the 3% case (used as the base case herein) seems likely to be close to the lower limit of ratios that would be worthwhile in practice. For example, the distances required for the maximum steepness to reduce below 20 kPa/s are approximately 575 m, 850 m and 1750 m for

volumetric ratios of 5%, 4% and 3% respectively. By comparison, a study of asymptotic values in Liu et al [22] shows that, for the assumed inviscid conditions, the ratios of 2% or less would never reduce the maximum steepness to below 20 Pa/s in tunnels of realistic length. Nevertheless, these smaller values could be considered as a means of, say, reducing the required lengths of dedicated extension regions at portals (especially at *exit* portals). For the larger ratios, the required length of tunnel in which the chambers would need to be provided reduces strongly with increasing chamber size. A possible method of taking advantage of the dependence on the volumetric ratio is raised in Section 5 below.

Figures-8(b,c) show the detailed shapes of wavefronts after travelling 1 km and 4 km. In all cases, the locus of the maximum steepness has migrated towards the effective toe of the wavefront and, for the 1% case, it has effectively reached the toe. Also, the bulk wave speed is seen to decrease with increasing volume ratio. In the absence of chambers, the mid-amplitude section of the 2 kPa amplitude wavefronts would travel about 3 m/s faster than the toe. In contrast, with volume ratios of 3% and 5%, it actually travels approximately 2.5 m/s and 5 m/s more slowly than the toe.

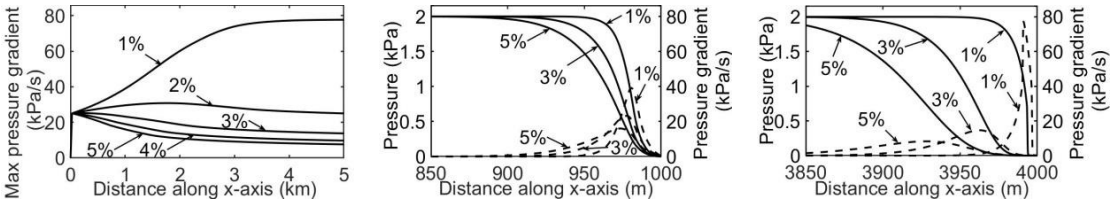

(a) Evolution of maximum gradient (b,c) Instantaneous profiles after 1 km & 4 km

Fig-8 Influence of chamber:tunnel volume ratio

(V_R = 1, 3 & 5%; K_1 depends on V_R; K_2 =0; K_1/K_{1c} = 2; wavefront = 2 kPa; 50 m)

4.4 Connector resistance

Figure-9 shows the evolution of the base case wavefront in tunnels with the base case chamber volume ratio (3%), but different connector resistances, namely the base case value K_1 = 1000 $m^{-1}s^{-1}$ and both half and twice this value. In practice, a change to the resistance implies a change in

geometry and the consequences for this on the corresponding value of the critical resistance will depend upon the particular geometry. Throughout Fig-9, $K_1/K_{1c} = 2$.

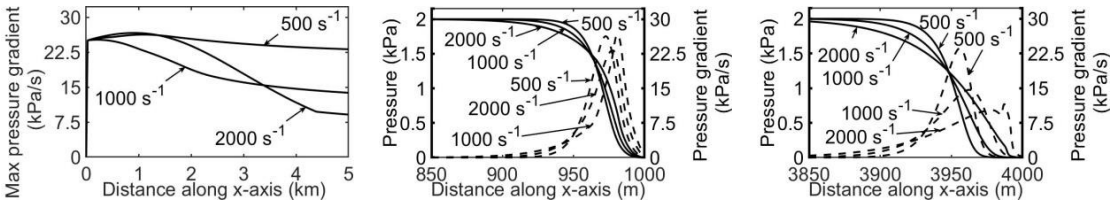

(a) Evolution of maximum gradient (b,c) Instantaneous profiles after 1 km & 4 km

Fig-9 Influence of linear-resistance connectors on evolving wavefront steepness

(V_R = 3%; K_1 = 500, 1000 & 2000 s^{-1}; $K_2 = 0$; $K_1/K_{1c} = 2$; wavefront = 2 kPa, 50 m)

Figure-9(a) shows a more complex dependence on the connector resistance than might be expected intuitively. During the first 1 km or so, the steepness reduces more rapidly when K_1 = 1000 $m^{-1}s^{-1}$ than with either larger or smaller values, indicating that an optimum value exists. At larger distances, however, the highest resistance connectors perform best. Further simulations (not shown) reveal that (i) the optimum resistance in the early stages is approximately 1200 $m^{-1}s^{-1}$ and (ii) at distances greater than about 4 km, the rapid reduction seen in Fig-9(a) for the K_1 = 2000 $m^{-1}s^{-1}$ case ceases and the three curves then continue in sequence, roughly parallel to each other.

The origins of the different behaviours at relatively small and large distances can be inferred from Figs-9(b),(c). In the early stages of propagation, the wavefront shape is governed primarily by the initiating cause – e.g. train nose entry or, in this paper, a prescribed boundary condition. In contrast, during the later stages of propagation, the shape has a nearly asymptotic state that depends primarily on the chambers and the wavefront amplitude. Higher-resistance connectors cause greater overall elongation of the wavefront than lower-resistance ones. However, if the resistance is too large, the chambers react too slowly and the leading part of the wavefront become steep – as for the K_1 = 2000 $m^{-1}s^{-1}$ connectors in Fig-9(c).

4.5 Quadratic resistance

As indicated in Section-2.1, connectors with non-linear resistance characteristics can cause over-damping at some flow rates, but under-damping at others. The consequences of this are illustrated in Fig-10, which compares four cases, all for the same upstream wavefront (2 kPa, 100 m) and the same chambers (V_R = 3%). The non-linear behaviour is characterised by the quadratic approximation defined in Section 2.1, using K_2 = 2000, 4000 and 8000 $m^{-1}kg^{-1}$. The base-case linear resistance shown in previous figures is included for comparison in Fig-10(a), but (to avoid clutter) not in (b) & (c).

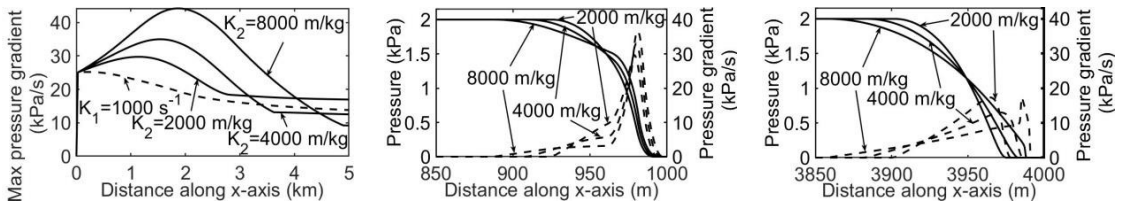

(a) Evolution of maximum gradient (b,c) Instantaneous profiles after 1 km & 4 km

Fig-10 Influence of quadratic-resistance connectors on evolving wavefront steepness

(V_R = 3%; K_1 = 0; K_2 = 2000, 4000 & 8000 $m.kg^{-1}$; wavefront = 2 kPa, 50 m)

The general behaviour broadly mirrors that shown in Fig-9 for linear-resistance connectors. However, the quadratic case is slow to respond; it allows the steepness of the leading part of the wavefront to increase strongly before decreasing. This behaviour is stronger for high-resistance connectors than for low-resistance ones although the high-resistances also perform even better than the linear base case after the wavefront has travelled sufficiently far.

When first seen, the behaviour illustrated in Figs-9(a) and 10(a) was not intuitively obvious to the authors. In the early stages of propagation, the effectiveness of the chamber decreases with increasing resistance whereas, in the later stages, the opposite is true. However, the explanation for this is easily deduced from the predicted wavefront shapes at 1000 m and 4000 m and also from numerous results (not shown) at intermediate distances and at larger distances. Initially, the maximum steepness is at the mid-point. In the early stages of propagation, the steepness ahead of this point increases and the steepness behind it decreases. As the wavefront propagates, the locus

of the transition between these two types of behaviour gradually migrates forward and eventually reaches the leading edge of the whole wavefront. In Fig-10(c), this process has already completed for the lower-resistance cases, but it has not quite completed for the highest-resistance case (although it does so before the wavefront has travelled another kilometre).

It follows that relatively low-resistance, linear connectors are best suited to short tunnels whereas relatively high-resistance, quadratic connectors are likely to be superior in longer tunnels.

4.6 Connector inertance

In all of the preceding simulations with linear resistance connectors, $K_1/K_{1c} = 2$ and, in practice, this ensures that the inertance of the connectors has little influence on the outcome. Over-damping such as this is likely to become a practical design requirement, but it is nevertheless useful to consider behaviour when the condition is not met. One purpose of this is simply to illustrate the influence of under-damping. A potentially more important purpose is to estimate how large the inertance can be without significantly compromising the effectiveness of chambers.

Figure-11 shows the potentially-strong influence of the ratio K_1/K_{1c} on the behaviour of the wavefront. The curves labelled '2' are the base case (i.e. $K_1/K_{1c} = 2$), which typifies the desired over-damped behaviour. This is compared with two underdamped cases in which the resistance K_1 is the same as in the base case, but the inertial coefficient is larger, giving $K_1/K_{1c} = 0.5$ and 0.25 respectively. The case of critical damping (i.e. $K_1/K_{1c} = 1$) is not shown in the Figs-11(b,c) because it is nearly indistinguishable from the base case except very close to the toe of the wavefront. Indeed, at 1km, the outcome for the under-damped case $K_1/K_{1c} = 0.5$ also differs only slightly from the base case - although the differences subsequently increase considerably.

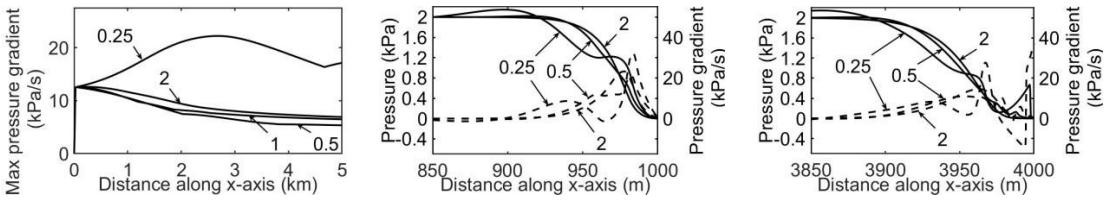

(a) Evolution of maximum gradient (b,c) Instantaneous profiles after 1 km & 4 km

Fig-11 Influence of connector inertance on evolving wavefront steepness

(V_R = 3%; K_1 = 1000 s^{-1}; K_2 = 0; K_1/K_{1c} = 0.25, 0.50 & 2.00; wavefront = 2 kPa, 50 m)

The importance of avoiding significant under-damping is illustrated clearly by the strong oscillations seen when K_1/K_{1c} = 0.25. These instantaneous profiles provide no direct information about the frequency of oscillation, but they demonstrate that it extends over the whole of the wavefront – although it is strongest close to the toe. For completeness, it is noted that the dominant wavelengths in the predicted profiles are in the order of one or two tunnel diameters and hence will not be predicted with high accuracy by 1-D analyses. However, that is not important for immediate purposes because such oscillations do not exist with suitably over-damped chambers.

5 POSSIBLE PRACTICAL APPLICATION

The principal focus of this paper is on the physical behaviour of wavefront propagation. It has been shown that suitably designed chambers and connectors have the potential not only to limit rates at which wavefronts steepen, but also to reduce the steepness of wavefronts that are initially very steep. This outcome is achievable with connectors that will ensure over-damped behaviour and that have linear resistance characteristics. Any design that satisfies these requirements would be acceptable in principle. The particular design illustrated in Fig-1b is considered in more detail in the Appendix.

5.1 Location in tunnel cross-section

An obvious issue for designers is how to provide space for the proposed chambers without also increasing the required cross-sectional area of the tunnel. One potential location is the region

beneath walkways along a tunnel. Another is the region below track level. The below-walkway region is likely to be smaller in bored tunnels than in cut-and-cover tunnels, whereas the opposite is true for the below-track region. If necessary, the possibility of increasing the overall cross-sectional area could be considered. Big increases would be ruled out on cost grounds, but small increases might pay for themselves by avoiding the need for other methods of preventing the emission of unacceptably large MPWs.

5.2 Maintenance

Another significant issue is the need to avoid maintenance issues or, more realistically, to reduce the need to acceptable levels. Ideally, there should be no moving parts and no requirement for external power. However, any connectors will necessarily be open to the tunnel, which is likely to be a dusty environment. The authors do not have relevant expertise in such matters as the avoidance of clogging of connector pores, so this issue is left as a subject for further investigation. It does not seem likely that methods developed for self-cleaning, non-porous surfaces in other applications in the construction field could be adapted to this purpose [28-30]. However, since only small masses of air will flow into and out of the chambers and the velocities of such flows will be small, it is plausible that low maintenance arrangements can be found.

5.3 Exit regions

In the above discussion, it is assumed that the air chambers are uniformly distributed and closely spaced. However, it does not follow that they must exist along the whole length of the tunnel. Indeed, the ability of the chambers to reduce large steepnesses rapidly (Fig-5) opens up the possibility of installing them only in the regions of tunnel adjacent to exit portals as assumed by Tebbutt et al [17]. In principle, wavefronts generated further upstream would be allowed to shorten indefinitely until reaching the region with chambers, in which they would rapidly elongate. The potential of this approach will increase strongly if larger chambers can be used, ideally much larger. This would require only a modest local increase in the tunnel cross-section so the implied increase in

construction costs might be smaller than the cost of portal extensions, giving financial as well as environmental benefits.

6 CONCLUSIONS

The propagation of wavefronts along tunnels with connections to multiple air chambers has been studied with a view to preventing the radiation of unacceptable pressure disturbances from tunnel portals. In contrast with previous studies of the influence of chambers, the possibility of resonance behaviour is explicitly avoided. It is shown that such chambers strongly counter the usual tendency of waves to steepen as they propagate and that, in tunnels of sufficient length, the maximum steepness of a wavefront becomes almost independent of its initial steepness. Instead, it depends upon the overall amplitude of the wavefront and on properties of the chambers and their connections to the tunnel. The preferred resistance characteristic of the connections have been shown to depend upon the tunnel length. For short tunnels, connectors with linear (laminar-like) resistance are suitable whereas, for longer tunnels, quadratic (turbulent-like) resistance can be more effective. Attention has focussed on chambers that are sufficiently compact to be modelled with good accuracy using bulk-volume approximations. Overall, it is concluded that, subject to meeting practical requirements unrelated to pressures and flows, the use of chambers could have the potential to eliminate the need for alternative counter-measures against unacceptable MPWs.

ACKNOWLEDGEMENTS

The authors are grateful to the following bodies that provided financial support for the project: (a) National Natural Science Foundation of China (grant no. 52002265), (b) China Scholarship Council (201806935055), (c) State Key Laboratory of Traction Power (grant no. TPL1904), (d) Scientific and Technological Innovation Programs of Higher Education Institutions in Shanxi (grant no. 2019L0251), (e) Natural Science Foundation of Shanxi Province, China (grant no. 201801D221224).

REFERENCES

[1] S. Ozawa, Countermeasures to reduce booms from exits of Shinkansen tunnels, Japanese Railway Engineering 24 (2) (1984) 2-5.

[2] S. Ozawa, T. Maeda, T. Matsumura, K. Uchida, H. Kajiyama, K. Tanemoto, Counter-measures to reduce micro-pressure waves radiating from exits of Shinkansen tunnels, studies of micro-pressure wave radiated from a tunnel exit, Proc. 7th Int. Symp. on Aerodynamics and Ventilation of Vehicle Tunnels 253 (1991).

[3] M. S. Howe, On the compression wave generated when a high-speed train enters a tunnel with a flared portal, J. Fluids Struct. 13 (1999) 481-498.

[4] T. Miyachi, S. Saito, T. Fukuda, Y. Sakuma, S. Ozawa, T. Arai, S. Sakaue, S. Nakamura, Propagation characteristics of tunnel compression waves with multiple peaks in the waveform of the pressure gradient , Proc. IMechE Part F: J Rail Rapid Trans. 230 (4) (2016) 1297-1308.

[5] X. Xiang, L. Xue, B. Wang, W. Zou, Mechanism and capability of ventilation openings for alleviating micro-pressure waves emitted from high-speed railway tunnels. Building and Environment 132 (2018) 245-254.

[6] S. Saito, Optimizing cross-sectional area of tunnel entrance hood for high speed rail, J. Wind Eng. Ind. Aerod. 184 (2019) 396-304.

[7] J. Burri, F. Zumsteg, Airshafts for the alleviation of pressure waves in tunnels of the new Swiss Rail 2000, 9th Int. Symp. Aerodynamics and Ventilation of Vehicle Tunnels, Aosta-Valley, 27 (1997) 289-299.

[8] H. Wang, A. E. Vardy, Influence of shaft:tunnel geometry on steep pressure waves, 17th Int. Symp. on Aerodynamics, Ventilation and Fire in Tunnels, ISAVFT. BHR Group Limited. (2017) 41-53.

[9] T. Aoki, A. E. Vardy, J. M. B. Brown, Passive alleviation of micro-pressure waves from tunnel portals, J. Sound Vib. 220 (5) (1999) 921-940.

[10] M. Nishimura, M. Kondo, K. Iwamoto, Y. Tsujimoto, Active attenuation of impulsive noise from a railway tunnel exit. Proceedings of Inter-noise 94, Yokohama (1994) 1383-1388.

[11] T. Fukuda, S. Nakamura, T. Miyachi, S. Saito, N. Kimura, M. Matsunuma, Countermeasure for reducing micro-pressure waves by spreading ballast on the slab-track in the tunnel, Quarterly Report of RTRI 59 (2) (2018) 121-127.

[12] T. Fukuda, S. Nakamura, T. Miyachi, S. Saito, N. Kimura, M. Matsunuma, Influence of ballast quantity on compression wavefront steepening in railway tunnels, Proc. IMechE Part F: J Rail Rapid Trans. 234 (6) (2020) 607-615.

[13] T. Maeda, T. Matsumura, M. Iida, K. Nakatani, K. Uchida, Effect of shape of train nose on compression wave generated by train entering tunnel, Proc. Int. Conf. Speed Up Technol. Railway Maglev Vehicles, Yokohama 2 (1993) 315-319.

[14] K. Kikuchi, M. Iida, T. Fukuda, Optimization of train nose shape for reducing micro-pressure wave radiated from tunnel exit, J. Low Frequency Noise Vib. Active Control 30 (1) (2011) 1-19.

[15] J. L. Peters, Tunnel optimized train nose shape, 10th Int. Symp. on Aerodynamics and Ventilation of Vehicle Tunnels, Boston, USA, (2000) 1015-1022.

[16] N. Sugimoto, Propagation of nonlinear acoustic waves in a tunnel with an array of Helmholtz resonators, J. Fluid Mech. 244 (1992) 55-78.

[17] J. A. Tebbutt, M. Vahdati, D. Carolan, J. P. Dear, Numerical investigation on an array of Helmholtz resonators for the reduction of micro-pressure waves in modern and future high-speed rail tunnel systems, J. Sound Vib. 400 (2017) 606-625.

[18] Th. Tielkes, H. J. Kaltenbach, M. Hieke, P. Deeg, M. Eisenlauer, Measures to counteract micro-pressure waves radiating from tunnel exits of DB's new Nuremberg-Ingolstadt high-speed line, Noise Vibr. Mitig. Notes on Numerical Fluid Mech. 99 (2008) 40-47.

[19] A. Sasoh, K. Matsuoka, K. Takayama, S. Hirano, S. Ono, Y. Makino, K. Ootsuka, Experiments on attenuation of weak shock waves in high-speed train tunnels, JSME International Journal Series B 41 (4) (1998) 814-821.

[20] S. Ozawa, K. Murata, T. Maeda, Effect of ballasted track on distortion of pressure wave in tunnel and emission of micro-pressure wave, Proc 9th Int. Symp. on the Aerodynamics and Ventilation of Vehicle Tunnels, BHR Group. 27 (1997) 935-947.

[21] A. E. Vardy, J. M. B. Brown, Influence of ballast on wave steepening in tunnels, J. Sound Vib. 238 (4) (2000) 595-615.

[22] F. Liu, D. Pokrajac, A. E. Vardy, Avoiding micro-pressure waves without building tunnel hoods, International Conference Tunnel Safety and Ventilation, Graz, 1-3 Dec (2020).

[23] H. Wang, B. Lei, H. Bi, Wavefront evolution of compression waves propagating in high speed railway tunnels, J. Sound Vib. 431 (2018) 105-121.

[24] K. Matsuo, T. Aoki, H. Kashimura, Y. Nonaka, Emission of propagating compression wave from an open end of a tube (1st report, Analytical study), Trans Japan Soc Mech Engrs Part B, 58(546), (1992) 331-337.

[25] K. Matsuo, T.Aoki, H. Kashimura, T. Yasunobu, S. Mashimo, Generation mechanism of impulsive wave emitted from high-speed railway tunnel exit, Proc 8th Int. Symp. on the Aerodynamics and Ventilation of Vehicle Tunnels, BHR Group, Liverpool, UK (1994) 199-209.

[26] H. Levine, J. Schwinger, On the radiation of sound from an unflanged circular pipe, Phys. Rev. 73 (4) (1948) 383-406.

[27] A. R. DaSilva, G. P. Scavone, A. Lefebvre, Sound reflection at the open end of axisymmetric ducts issuing a subsonic mean flow: A numerical study, J. Sound Vib. 327 (2009) 507-528.

[28] Y. Paz, Z. Luo, L. Rabenberg, A. Heller, Photo oxidative self-cleaning transparent titanium dioxide films on glass, J. Mater. Res. 10 (11) (1995) 2842-2848.

[29] K. Liu, L. Jiang, Bio-inspired self-cleaning surfaces, Annual Review of Materials Research 42 (2012) 231-263.

[30] P. Ragesh, V. A. Ganesh, S. V. Nair, A. S. Nair, A review on 'self-cleaning and multifunctional materials', J. Mater. Chem. A 2 (2014) 14773-14797.

APPENDIX: INDICATIVE CONNECTORS

In the main body of the paper, the connectors are represented generically by their resistance and inertial characteristics. One notionally possible way of achieving the desired properties is now described. It is not intended as a formal proposal for actual design. Instead, the purpose is to demonstrate that the required properties are achievable. The example is presented for the case of linear resistance.

The chosen example is illustrated in Fig-1b. It represents a small selection of thousands of small tubes per metre length of tunnel. Suppose that the total cross-sectional area of flow through the tubes is equivalent to 0.1 m^2 per metre along the tunnel axis. Further suppose that the tube length is 0.1 m (perhaps corresponding to the thickness of a concrete wall). The overall surface area required to achieve this will depend upon the packing configuration of the tubes. Thus, if the array is distributed uniformly along the tunnel, the overall surface area array might be equivalent to a continuous slot with a width of, say 0.2 m.

Figure-12 illustrates the dependence of K_1 on the diameter of the tubes. The curve labelled K_{1c} shows the value of K_1 corresponding to a critically-damped response to a sudden change in pressure from one steady value to another. For all tube diameters less than about 1 mm, the true response will be over-damped and, for diameters smaller than about 0.3 mm, the ratio K_1/K_{1c} exceeds 10. This implies strong over-damping. For practical purposes, this corresponds to almost wholly resistive behaviour, thereby more than satisfying the second of the above key requirements.

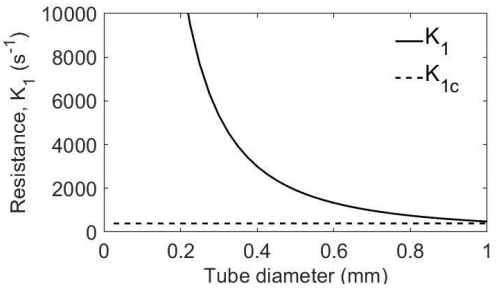

(a) Linear resistance parameter K_1

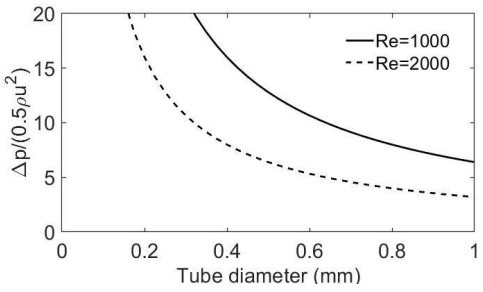

(b) Linear resistance scaled by $½\rho U^2$

Fig-12 Resistive behaviour in multiple parallel-tube connectors (L_e = 100 mm)

In the simulations presented above, the optimum resistance is generally in the range $500 < K_1 < 5{,}000$ $m^{-1}s^{-1}$. For the connection diameters in this illustration, all of this range is above the critical value of K_{1c}, namely 394 $m^{-1}s^{-1}$, so oscillatory behaviour would be avoided in all cases considered. At the upper end of the range, the resistance will dominate. At the lower end, inertia will have a small proportional influence, increasing the effective resistance during the period when flow through the connectors is accelerating and reducing it when the flows are decelerating. These periods coincide approximately with the periods of increasing and decreasing steepness of the propagating wavefront in Fig-6(b).

Although Fig-12(a) confirms that the desired range of K_1 is consistent with ensuring over-damped behaviour, it implicitly assumes that the implied linear resistance is physically possible. In principle, even if the flow along a tube itself is laminar, the overall resistance will not be wholly linear because account also needs to be taken of local losses at inlet and outlet. This matter is addressed in Fig-12(b) which compares the pressure difference in laminar flow along a tube with the pressure difference $½\rho U^2$ required for flow to enter the tube. The graphs are applicable for Reynolds numbers of 1,000 and 2,000, which is close to the expected upper limit of laminar flow. By inspection, the linear behaviour dominates at sufficiently small diameters, but the quadratic behaviour is increasingly important at larger diameters.

These results show that, for tube diameters smaller than about 0.4 mm, the behaviour of the connectors would be strongly over-damped and their resistance would be approximate linear. This corresponds to values of the resistance parameter K_1 exceeding approximately 3,000 $m^{-1}s^{-1}$, which is within the desired range. With larger diameters – up to about 1 mm, similar qualitative behaviour would be obtained, but the detailed behaviour would correspond less closely to that for strongly damped flows with wholly linear resistance.

Declaration of interests

☒ The authors declare that they have no known competing financial interests or personal relationships that could have appeared to influence the work reported in this paper.

☐The authors declare the following financial interests/personal relationships which may be considered as potential competing interests:

CRediT author statement

Influence of air chambers on wavefront steepening in railway tunnels

Liu, Vardy, Pokrajac

Feng LIU:

Software, Validation, Investigation, Reviewing, Funding acquisition

Alan VARDY

Conceptualisation, Methodology, Validation, Supervision, Writing – original draft

Dubravka POKRAJAC

Supervision, Methodology, Project administration, Software, Validation, Reviewing